ISSN (e): 2250 – 3005 || Volume, 06 || Issue, 11|| November – 2016 ||
International Journal of Computational Engineering Research (IJCER)

Passively Flapping Dynamics of a Flexible Foil Immersed in the Wake of a Cylinder

Dibo Dong[1], Weishan Chen, Zhenxiu Hou, Zhenbo Han
[1]State Key Laboratory of Robotics and System Harbin Institute of Technology Harbin, Heilongjiang Province, China.

ABSTRACT

Passive dynamics of flexible body in the von Kármán vortex is complicated and has not yet been well understood. In this work we numerically studied the passive flapping motion of an inverted flexible foil pinned in the wake of a rigid circular cylinder by an robust fluid structure interaction framework. The non-dimensional parameters are Reynolds number and distance between the cylinder and pinned-point of the foil. Simulation results show that the flexible foil can extract energy from the vortex street and be induced to vibrate periodically. It is revealed that the foil's motion patterns can be divided into two categories: inverted flapping and forward flapping, which depended on the cylinder-foil distance. Both the cylinder and foil experiences a drag reduction, the foil can even obtain thrust in inverted flapping mode. Compared with a single one in the same uniform flow, the foil's flapping frequency here is smaller but its amplitude is greater. This work would help us to elucidate the energy-saving mechanism of fish swimming and inspire the promising applications in marine engineering.

Keywords: *flow control, elastic plate; passively flapping, fluid-structure interaction.*

I. INTRODUCTION

The interaction between a rigid structure and a flexible body is a common phenomenon, like fishes swimming behind a ship or staying in the wake of a stationary structure. Fishes may take advantage of the interaction to save energy and lift efficiency. Two rigid bodies arranged in tandem, the downstream one enjoys a drag reduction [1]. Recently, the interaction between flexible bodies has been widely studied by simulations and experiments [2, 3]. For two tandem flexible bodies, the downstream will suffer a drag increase, which is opposite to the situation of two tandem rigid bodies. The interaction of coupled rigid and flexible bodies may be much different. Interaction between a upstream flexible filament and a downstream rigid cylinder is investigated in [4]. Reference [5] studied the effect of a thin wire placed in the wake of a rigid cylinder. In this paper, we places a flexible foil at the downstream of a rigid cylinder to study the interaction between rigid and flexible bodies in a viscous flow numerically. An immersed boundary-lattice Boltzmann method is adopted to carry out the simulations.

II. COMPUTATIONAL MODEL

A schematic diagram of the cylinder-foil system is shown in Fig. 1. A thin foil with length L is placed in downstream of a rigid circular cylinder with diameter d. The foil is considered as a two-dimensional thin beam with a simply supported boundary condition at the leading-edge. Both the center of the cylinder and the leading-edge of the foil are fixed at the center line of the fluid domain, the trailing-edge of the foil is free. The minimum distance between the cylinder and the leading-edge of the foil is the cylinder-foil distance D_s. Here we introduce a non-dimensionalize cylinder-foil distance ratio defined as $D = D_s/d$. The incoming flow is parallel to the X-axis with a velocity of U_∞.

The problem on a rigid body and a flexible foil immersed in a viscous flow is solved by the IB-LBM [6]. The fluid is discretized by a regular Cartesian lattice, the foil is discretized by a group of Lagrangian coordinate markers. The viscous fluid is govern by the incompressible Navier–Stokes and continuity equations:

$$\frac{\partial \boldsymbol{v}}{\partial t} + \boldsymbol{v} \cdot \nabla \boldsymbol{v} = -\nabla p + \frac{1}{Re} \nabla^2 \boldsymbol{v} + \mathbf{f} \,, \tag{1}$$

$$\nabla \cdot \boldsymbol{v} = 0 \,. \tag{2}$$

p is the pressure of the fluid, ρ is the fluid density, $\boldsymbol{v}$ =(v, u) is the fluid velocity as a function of time $t = L / U_\infty$. Re is the Reynolds number defined as $Re = U_\infty d / \mu$, μ is the fluid dynamic viscosity. The added momentum force **f** represents the force exerted by the structure on the fluid. The dynamics of the foil is governed by the equation:

$$\rho_l \frac{d^2\mathbf{X}}{dt^2} = \frac{d}{ds}\left(T\frac{d\mathbf{X}}{ds}\right) - K\frac{d^4\mathbf{X}}{ds^4} - \mathbf{F} = 0 \ . \tag{3}$$

ρ_l is the linear density of the foil, $\mathbf{X} = (X, Y)$ represents the position of the foil markers. s represents the Lagrangian coordinate along the foil. $T = T_c / \rho U_\infty^2 L$ is the tension. T_c (s, t) is the tension within the foil which determined by the markers

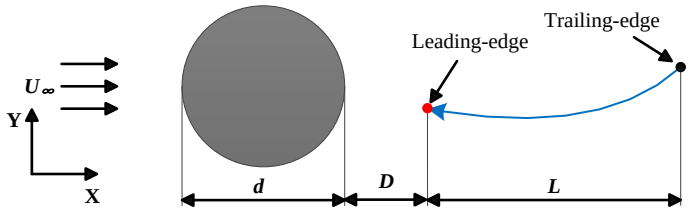

Fig. 1 Schematic diagram of the cylinder-foil system.

position **X**. K is the bending stiffness defined as $K = EI / (\rho U_\infty^2 L^3)$, EI is the bending rigidity of the foil. **F** is the hydrodynamic force exerts on the fluid by the foil which defined on the foil markers. The foil is considered to be inextensible, which provided by:

$$\frac{d\mathbf{X}}{ds}\cdot\frac{d\mathbf{X}}{ds} = 1 \ . \tag{4}$$

The boundary condition for the foil is:

$$\mathbf{X} = \mathbf{X}_0, \ \frac{d^2\mathbf{X}}{ds^2} = 0 \tag{5}$$

for the leading-edge,

$$T = 0, \ \frac{d^2\mathbf{X}}{ds^2} = 0 \tag{6}$$

for the trailing-edge. The momentum force $\mathbf{f} = (f_x, f_y)$ can be calculated by:

$$\begin{cases} \mathbf{f}(\mathbf{x},t) = \dfrac{1}{\Delta t}\Phi\, ds \\ \Phi = \displaystyle\int_\Gamma \left(\boldsymbol{U}(\mathbf{X}(s),t) - \int_\Omega \boldsymbol{v}(\mathbf{y})\delta(\mathbf{y} - \mathbf{X}(s)d\mathbf{y}) \right) \delta(\mathbf{x} - \mathbf{X}(s)) \end{cases} \tag{7}$$

Γ is boundary of the foil markers, Ω denotes the domain of the fluid. **x** denotes the coordinate of the Cartesian lattice of the fluid. $\boldsymbol{U}$ represents the velocity of the foil marker at **X**. $\boldsymbol{v}$ represents the fluid velocity field. δ is a mollifier [7] to perform the convolution which defined as:

$$\delta(d) = \begin{cases} \dfrac{1}{6}\left(5 - 3|d| - \sqrt{-3(1-|d|)^2 + 1}\right) & 0.5 \le |d| \le 1.5 \\ \dfrac{1}{3}\left(1 + \sqrt{-3d^2 + 1}\right) & |d| \le 0.5 \\ 0 & \text{ohterwise} \end{cases} \ . \tag{8}$$

Where d represents the distance between the Lagrangian coordinate $s \in \Gamma$ and the lattice coordinate $\mathbf{x} \in \Omega$. As shown in Fig. 2, by placing the tension points between each foil markers, equation (3) and (4) can be discretised into a staggered fashion:

$$\begin{cases} \dfrac{\mathbf{X}^{n+1} - 2\mathbf{X}^{n} + \mathbf{X}^{n-1}}{\Delta t^{2}} = \dfrac{\left[D_s (T^{n+1} D_s \mathbf{X}^{n+1}) \right] - K D_{ssss} \mathbf{X}^{n} - \mathbf{F}^{n}}{\rho_l} \\ D_s \mathbf{X}^{n+1} \cdot D_s \mathbf{X}^{n+1} = 1 \end{cases} \tag{9}$$

Δt is the increment of time. D_s denotes the standard second-order center finite difference for s. The lattice Boltzmann equation (LBE) [8] is used to solve the fluid instead of the Navier–Stokes equations because of its efficiency. The LBE with the BGK approach is:

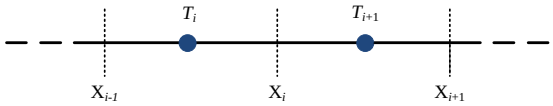

Fig. 2 Discretisation grid of the plate in a staggered form. Blue circles represents tension points, between tension points are coordinate markers.

$$f_i(\mathbf{x} + \mathbf{e}_i \Delta t, t + \Delta t) - f_i(\mathbf{x}, t) = -\frac{\Delta t}{\tau}\left(f_i(\mathbf{x}, t) - f^{eq}(\mathbf{x}, t) \right) + \Delta t \mathbf{F}_i \tag{10}$$

Where τ is a relaxation time which related to the dynamic viscosity as $\mu = (\tau - 1/2)/3$. $f_i(\mathbf{x}, t)$ denotes the distribution function with respect to the fluid particles at position $\mathbf{x}$ and time t, $\mathbf{e}_i$ is the discrete particles velocity which is shown in Fig. 3. The subscript i is the directions of the fluid particles, in this model, $\mathbf{e}_i$ is defined as:

$$\boldsymbol{e}_i = \begin{pmatrix} 0 & 1 & -1 & 0 & 0 & -1 & 1 & -1 & 0 \\ 0 & 0 & 0 & 1 & -1 & -1 & -1 & 1 & 0 \end{pmatrix} (i = 0, 1, \ldots, 8) \tag{11}$$

$f^{eq}(\mathbf{x}, t)$ is the equilibrium function which can be obtained by:

$$f^{eq}(\mathbf{x}, t) = \rho \omega_i \left[1 + \frac{\mathbf{e}_i \cdot \boldsymbol{v}}{c_s^2} + \frac{(\mathbf{e}_i \cdot \boldsymbol{v})^2}{2 c_s^4} - \frac{\boldsymbol{v}^2}{2 c_s^2} \right] \tag{12}$$

c_s is the sound velocity and ω_i is the weighting coefficients. The discretised force $\mathbf{F}_i$ relates to the $\mathbf{f}$ is defined as follows:

$$\mathbf{F}_i = \omega_i \left(1 - \frac{1}{2\tau} \right) \left[\frac{\mathbf{e}_i - \boldsymbol{v}}{c_s^2} + \frac{\mathbf{e}_i \cdot \boldsymbol{v}}{c_s^4} \mathbf{e}_i \right] \cdot \mathbf{f} \tag{13}$$

the macroscopic quantities of density ρ and $\boldsymbol{v}$ can are obtained by:

$$\rho = \sum_i f_i \tag{14}$$

$$\rho \boldsymbol{v} = \sum_i f_i \mathbf{e}_i + \frac{\Delta t}{2} \mathbf{f} \tag{15}$$

The dimensionless mass ratio of the foil is defined as: $M = \rho_l / (\rho L)$, the dimensionless drag coefficient for the foil and cylinder is: $C_d = 2F_d / \rho U_\infty^2 L$ and $C_d = 2F_d / \rho U_\infty^2 d$. The dimensionless lift coefficient is defined as $C_l = 2F_l / \rho U_\infty^2 L$ and $C_l = 2F_l / \rho U_\infty^2 d$. F_d and F_l are the hydrodynamic force along the X-axis and Y-axis respectively.

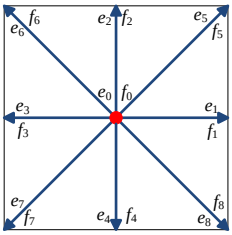

Fig. 3 The distribution function and the discrete particles velocity.

The flapping amplitude A_f is defined as the displacement along the Y-axis of the trailing-edge, and $A = A_T / L$ is the dimensionless flapping amplitude. The flapping frequency of the foil and the vortex shedding frequency of the cylinder are represented by f.

The X-axis length for the fluid domain is 80d and the Y-axis length is 40d. The center of the cylinder is placed 20d away from the inlet of the fluid domain. The position of the foil is decided by the distance ratio D. The foil is parallel to the X-axis at the beginning of the simulation. The foil markers and the Cartesian lattice is in uniform distribution. Both the distance between two neighboring markers and the lattice spacing is set to 0.01. The diameter d and the foil length L is set to $d = L$, so the size for the fluid domain is 2000 × 1500. Unless other stated, the Reynolds number is Re = 100 , the mass ratio of the foil is M = 0.3 and the bending stiffness is K = 10^{-4}. In such parameters, the flexible foil can flap in a stable motion periodically as the simulation results showed. All the results analyzed below are obtained by these stable periods.

III. RESULT AND DISCUSSION

Two categories of the foil's motion patterns are founded by changing the cylinder-foil distance: inverted flapping and forward flapping, as shown in Fig. 4. When the cylinder-foil distance is small enough, the foil will flap towards the opposite direction of the incoming flow. The free end of the foil will move upstream and go across the pinned-point, then gets into a stable flapping motion with the free end pointing to the upstream cylinder. There is a backflow zone behind the cylinder, as shown in Fig. 5, the flow speed of this area is contrary to the streamwise [9], and the pressure is low. The foil in the backflow zone will experiences a force along the negative direction of the X-axis, and finally the foil will turn around and flap towards the upstream direction. With the increasing of the cylinder-foil distance, the foil's motion patterns will turn to the forward flapping mode, which the trailing-edge points to the downstream. The crucial cylinder-foil distance of the mode shift is decided by the length of the backflow zone. Fig. 4 plots the flapping pattern of the inverted flapping mode at D = 2.1 and the forward flapping mode at D = 3.5. The flapping amplitude and the Y-velocity of the trailing-edge in the inverted flapping mode is obviously smaller than that of the forward flapping mode. From Fig.5 (e) we can see the flapping trajectory of the trailing-edge at D = 2.1 is not fully symmetrical about the centre line of the fluid. We can find the reason in Fig. 6 which plots the stream lines for the two different flapping mode. For D = 2.1, the backflow zone deviates to one side of the cylinder, which has a attraction for the foil and lead to the unsymmetrical of the flapping motion of the foil. The backflow zone at D = 2.1 is much bigger than that at D = 3.5, we can infer that the exists of the foil may has a influence on the shape of the backflow zone.

The average drag coefficient and the amplitude of lift coefficient and the flapping frequency of the foil are shown in Fig. 7. All the figures are divided into two parts: part I and part II corresponding to the inverted flapping mode and forward

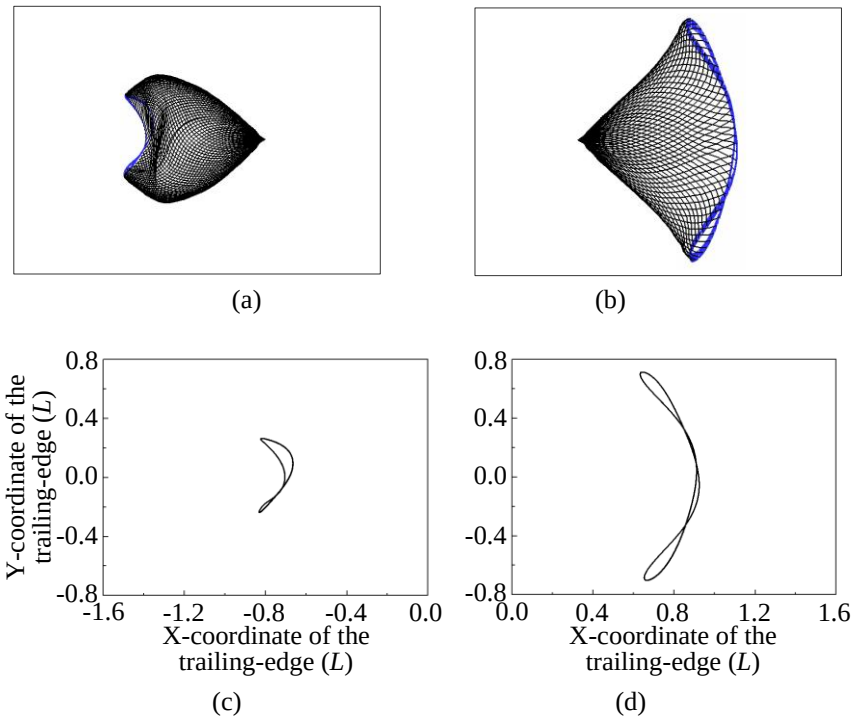

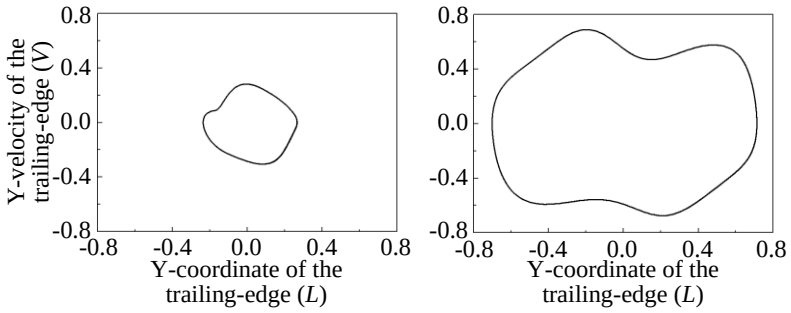

(e) (f)

Fig. 4 The flapping patterns of the foil, the flapping trajectory and the phase plot of the of the trailing-edge of the foil at *Re* = 100, origin of coordinates for flapping trajectory and phase plot is set at the leading-edge and trailing-edge respectively, with (a), (c), (e) *D* = 2.1 and (b), (d), (f) *D* = 3.5.

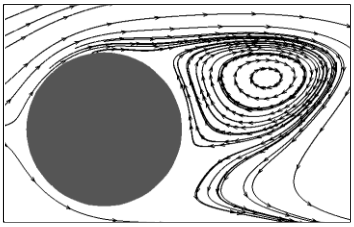

Fig. 5 The backflow zone

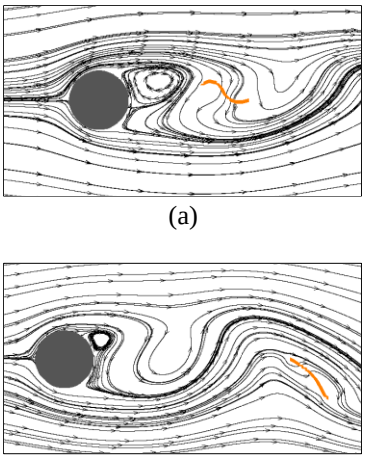

(a)

(b)

Fig. 6 Stream lines for (a) *D* = 2.1 and (b) *D*= 3.5

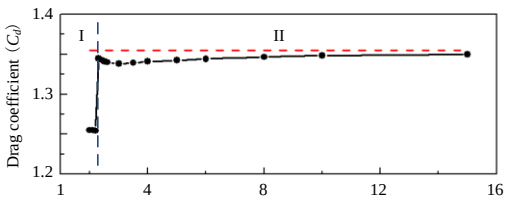

(a) Cylinder-foil distance ratio (*D*)

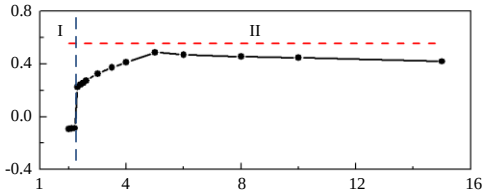

(b) Cylinder-foil distance ratio (*D*)

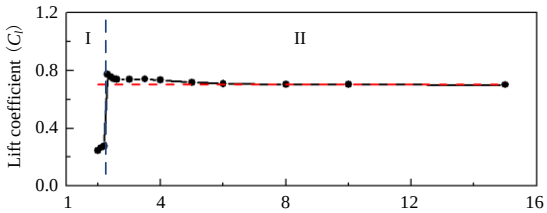

(c) Cylinder-foil distance ratio (*D*)

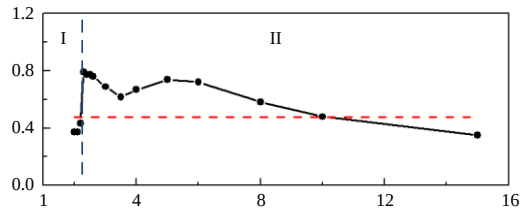

(d) Cylinder-foil distance ratio (*D*)

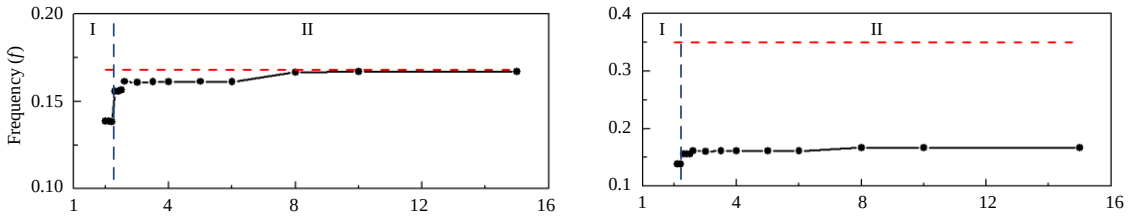

(e) Cylinder-foil distance ratio (D) (f) Cylinder-foil distance ratio (D)

Fig. 7 The average drag coefficient C_d, the amplitude of lift coefficient C_l, the flapping frequency of the foil and the vortex shedding frequency of the cylinder versus the cylinder-foil distance ratio with (a), (c), (e) for the cylinder and (b), (d), (f) for the foil.

flapping mode respectively. The range $D \leq 2.2$ corresponds to the inverted flapping mode (part I), drag on the foil is negative, drag on the cylinder is much smaller than that of the single cylinder, both of foil and cylinder experiences a significant drag reduction. The tendency of the amplitude of lift and vortex shedding frequency for the cylinder is similar with that of drag. The range $D \geq 2.3$ corresponds to the forward flapping mode (part II). Average drag and the amplitude of lift of the cylinder is much larger than that of the inverted flapping mode. The cylinder still experiences a drag reduction but the amplitude of lift exceeds the single cylinder. With the increasing of the cylinder-foil distance, all this three parameters of the cylinder approach to that of the single cylinder, at $D \geq 8.0$, they are almost equal to those of the single cylinder. Drag and lift on the foil increases sharply when the foil's motion patterns shift too. At the range $2.3 \leq D \leq 4.0$, there is still a obvious drag reduction on the foil, when $D \geq 5.0$, the drag reduction vanishes. The amplitude of lift coefficient of the foil goes a opposite tendency with that of the drag coefficient. At $2.3 \leq D \leq 8.0$, the amplitude of lift is larger than the single foil case. The vortex shedding frequency of the cylinder decreases because of the exists of the foil, especially when the cylinder and foil are close to each other. The downstream foil can be treat as a barrier and a wake splitter which inhibits the flow, from Fig. 6 we can see the stream lines around the foil are distorted. This hinders the vortex shedding and also enlarges the size of the backflow zone. This will lead to a drag reduction of the upstream cylinder. More closer the foil to the cylinder, more significant the influence is, which conforms to the results shown in Fig. 7.

Flapping frequency of the foil is much smaller than that of the single foil, and always equal to the vortex shedding frequency even the distance ratio increase to $D = 15.0$. The flapping amplitude of the trailing-edge of the foil shown in Fig. 8 is much larger than the single foil case in the forward flapping mode. We can infer that the vortexes shedding by the cylinder has a strong influence on the flapping motion of the downstream foil. As shown in Fig. 7 and 8, When $D \geq 8.0$, the influence of the foil on the cylinder is almost gone, but even at $D = 15.0$, the cylinder still changes the motion of the foil.

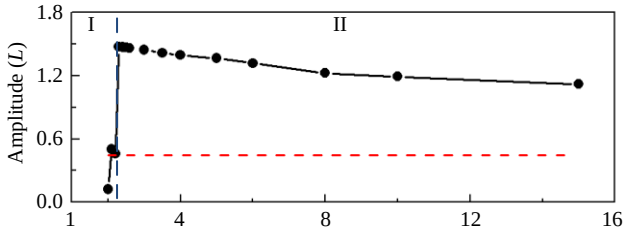

Fig. 8 The flapping amplitude of the trailing-edge of the foil versus the cylinder-foil distance ratio.

For a more detailed analysis, the time history of Y-position of trailing-edge, drag coefficient C_d of the foil and lift coefficient C_l of the foil at $D = 2.1$ and $D = 3.5$ are shown in Fig. 9. At time point A and C, drag on the foil reaches its maximum, the trailing-edge Y-position is near zero, at time point B, drag reaches its minimum, the Y-position is near its peak. But the situation for time point D, E and F is just opposite. Maximum drag corresponds to the peak of Y-displacement of the trailing-edge and minimum drag corresponds to the zero point of Y-displacement. Lift at point D to F shows that the peak of lift happens when the Y-displacement of trailing-edge is near zero. But due to the unsymmetrical of the flapping motion at $D = 2.1$, the lift at point A and C are not exactly zero. The different corresponding relationship in the two motion patterns shows that the cylinder influent the downstream foil in two different ways. Fig. 10 shows the vorticity contours at time point A, B, D and E.

We can see from the vorticity contours at time point A and B, between foil and cylinder is small that the foil is in the area the cylinder vortexes doesn't start to shed. The foil is in between of the positive and negative vorticity, the vorticity around the foil is opposite with the vorticity generated by the cylinder because of the inverted flapping of the foil. The contact of two kinds of opposite vortexes will decrease the vorticity around the

foil and inhibits the flapping motion. The vorticity contours at time point D and E shows that the downstream foil encounters the vortexes shedding by the cylinder. The positive vorticity at one side of the foil merges with the upstream positive vortex, and the negative vorticity at the other side of the foil decreases, this makes the positive vorticity around the foil is much larger than the negative vorticity, and it's the same situation when the foil contours the upstream negative vortex, which lead to the increase of the flapping amplitude of the foil. This interaction also induce the foil to vibrate with the same frequency the cylinder sheds the vortex.

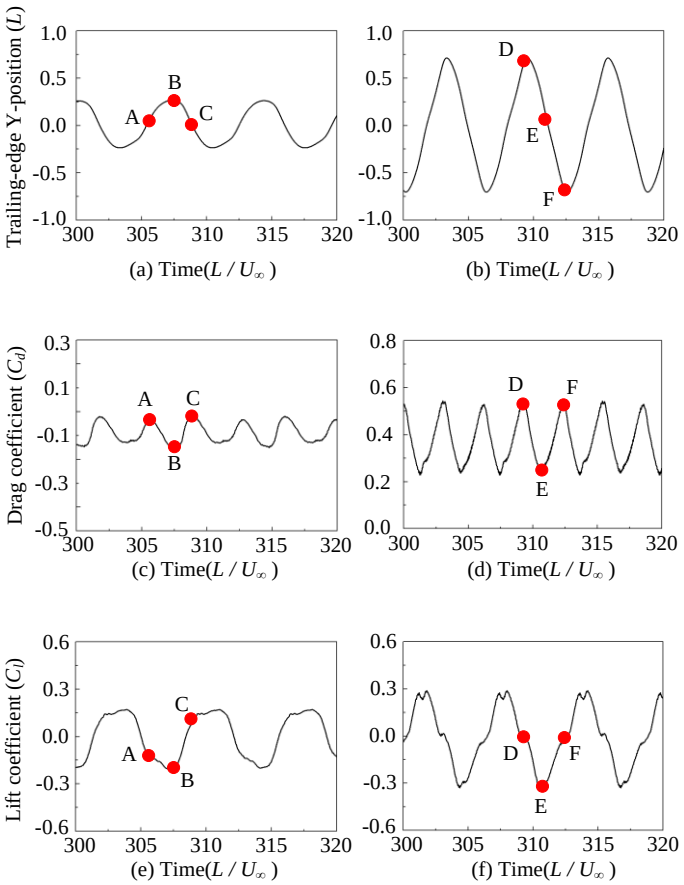

Fig. 9 Time history of Y-position of trailing-edge, drag coefficient C_d of the foil and lift coefficient C_l of the foil with (a), (c), (e) at D = 2.1 and (b), (d), (f) at D = 3.5. Point A to E corresponding to the two peaks of C_d and minimum value of C_d within a cycle.

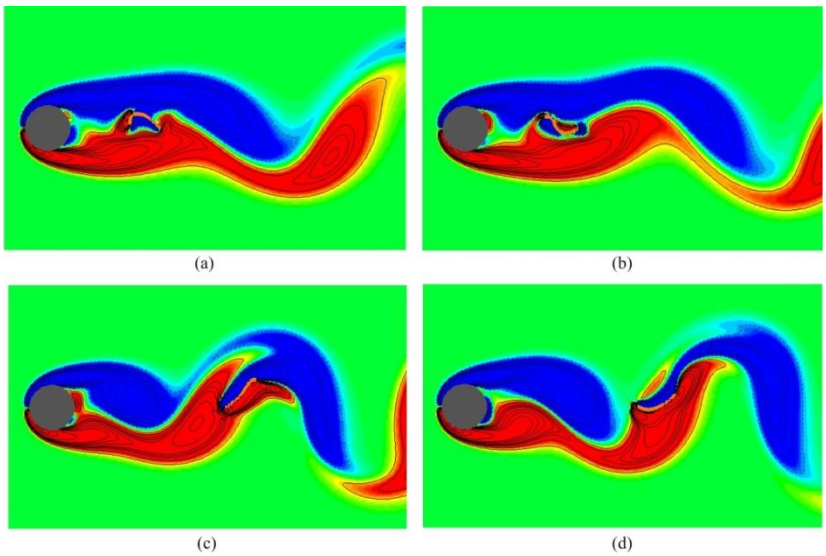

Fig. 10 Vorticity contours at time point (a) A, (b) B ,(c) D and (d) E

IV. CONCLUSION

The passive dynamics of flexible foil in the downstream of a rigid cylinder has been studied by the immersed boundary-lattice Boltzmann method. Simulation results show that the cylinder has a strong influence on the downstream foil. By varying the cylinder-foil distance, the foil's motion patterns can be divided into two categories: inverted flapping mode and forward flapping mode. In the inverted flapping mode, the foil will invert and flap towards the upstream cylinder because of the attraction of the backflow zone. In the forward flapping mode, the amplitude of the foil is greater but the frequency is smaller compared with a single one in the same uniform flow. Both the cylinder and foil experiences a drag reduction. Compared with a single one in the same uniform flow, the foil's flapping frequency here is smaller but its amplitude is greater. The flexible foil can extract energy from the vortex street and be induced to vibrate periodically. Exists of the foil also change the dynamics of the cylinder. The foil can be treated as a barrier and a wake splitter which inhibits the vortex shedding and enlarges the size of the backflow zone when the cylinder-foil distance is small. This also leads to a drag reduction of the upstream cylinder. The interactions between the rigid cylinder and the flexible foil would help us to understand the energy-saving mechanism of fish swimming behind a structure and inspire the promising applications in marine engineering.

ACKNOWLEDGMENT

We would like to acknowledge sincerely the grant from National Natural Science Foundation of China (No. 50905040) and the Fundamental Research Funds for the Central Universities.

REFERENCES

[1] Y. Koda, and F. Lien, "Aerodynamic effects of the early three-dimensional instabilities in the flow over one and two circular cylinders in tandem predicted by the lattice Boltzmann method," Computers & Fluids, vol. 74, pp. 32-43, March 2013.

[2] E. Uddin, W. Huang, and H. Sung, "Interaction modes of multiple flexible flags in a uniform flow," J. Fluid Mech, vol. 729, pp. 563-583, July 2013.

[3] W. Zhao, et al, "Theoretical and experimental investigations of the dynamics of cantilevered flexible plates subjected to axial flow," Journal of Sound and Vibration, vol. 331, no. 3, pp. 575-587, January 2012.

[4] F. Tian, H. Luo, L. Zhu, and X. Liu, "Interaction between a flexible filament and a downstream rigid body," Physical Review E, vol. 82, no. 2, pp. 026301, August 2010.

[5] I. Yildirim, C. Rindt, and A. Steenhoven, "Vortex dynamics in a wire-disturbed cylinder wake," Physics of Fluids, vol. 22, no. 9, pp. 094101, September 2010.

[6] J. Favier, A. Revell and A. Pinelli, "A Lattice Boltzmann–Immersed Boundary method to simulate the fluid interaction with moving and slender flexible objects," Journal of Computational Physics, vol. 261, pp. 145–161, March 2014.

[7] A. Roma, C. Peskin, and M. Berger, "An adaptive version of the immersed boundary method," Journal of Computational Physics, vol. 153, no. 2, pp. 509–534, August 1999.

[8] O. Malaspinas, N. Fietier, and M. Deville, "Lattice Boltzmann method for the simulation of viscoelastic fluid flows," Journal of Non-Newtonian Fluid Mechanics, vol. 165, no. 23, pp. 1637-1653, December 2010.

[9] J. Eldredge, and D. Pisani, "Passive locomotion of a simple articulated fish-like system in the wake of an obstacle," Journal of Fluid Mechanics, vol. 607, pp. 279-288, July 2008.